Journal of the Brazilian Society of Mechanical Sciences and Engineering (2023) 45:362
https://doi.org/10.1007/s40430-023-04282-y

TECHNICAL PAPER

Improving the micromixing and thermal performance using a novel microreactor design

Ahmed H. El-Shazly[1,2] · Maud Gracious Fuko[1] · Atusaye G. Sichali[1]

Received: 23 September 2022 / Accepted: 17 May 2023 / Published online: 13 June 2023

Abstract

Mixing and thermal performance are crucial factors to consider in many chemical processes. Microreactor performance is frequently evaluated using the Villermaux–Dushman test reaction. The Villermaux–iodide/iodate Dushman's test reaction method and thermal camera were used in this study to investigate the mixing capabilities of multistage Y-arrow-shaped (Y-A) micromixers at laminar flow. Test solutions were fed through a 500-µm uniform diameter multistage Y-A-shaped microreactor with varied Y angles of 45° and 60°, and different volume flow rates of 100 to 600 ml/h and three different concentration sets 1, 1c, and 2b. A comparison of the absorbance values, segregation index of the products, and micromixing time made by the two mixers revealed that the 45° multistage Y-A-shaped micromixer offered the best mixing performance at volume flow rates under 600 mL/h. For thermal mixing efficiencies, the 45° microreactors had higher output temperatures as compared to the 60° microchannel. In this project, a basis for the design of a microreactor thermal performance was further provided through computational fluid dynamics (CFD) simulation. The effects of microreactor design parameters on fluid flow and mixing efficiency were studied by CFD simulation whose results showed that the angle of the multistage Y-A-shaped microreactor had a significantly positive effect on the mixing efficiency. Based on the simulation results, the splitting collision mechanism is discussed, and other recommendations have been obtained. Additionally, the experimental results showed that the mixing efficiency for the two microreactors was good for both 60° and 45° microreactors with the segregation index of range 0.007–0.02 and 0.002–0.018, respectively, which showed better performance than other fabricated designs of similar nature.

Keywords Micromixing · Computational fluid dynamics · Thermal efficiency · Segregation index

1 Introduction

Micromixing is a crucial process in any chemical reacting system as it increases contact between reacting species; as a result, it also reduces reaction time. Numerous chemical, petrochemical, and pharmaceutical applications benefit from the increased surface-to-volume ratio that microreactor devices' small-scale flow channels provide [1]. Microreactors devices offer several benefits over conventionally sized systems. Microreactors make it possible to analyze and use fewer amounts of materials, chemicals, and reagents, which lowers overall application costs. Because of its small size, several processes may be carried out, simultaneously cutting down on experimentation time. Additionally, they provide significant parameter control and great data quality, enabling process automation while maintaining performance. They are capable of processing and analyzing materials with just minimal sample handling [2]. The majority of microreactors operate at extremely low Reynolds number regimes; as a result, the flow created in these microchannels is laminar, and species mix mostly due to molecular diffusion, which is a naturally slow process and the micromixing efficiency is low. As a result, there is a need to develop effective microreactor mixing strategies to boost microreacting processes' throughput [3].

The diffusion resistance governs the rate of reactions. This means that long channels are employed which are costly due to high pressure drops. Thus, to optimize the process,

Technical Editor: Daniel Onofre de Almeida Cruz.

✉ Maud Gracious Fuko
maud.fuko@ejust.edu.eg

[1] Chemical and Petrochemicals Engineering Department, Egypt-Japan University of Science and Technology, New Borg El-Arab City, Alexandria, Egypt

[2] Chemical Engineering Department, Faculty of Engineering, Alexandria University, Alexandria 21544, Egypt

more innovative work has been done by the researchers even at laminar flow regimes. Some of the methods include the use of external energy sources, the use of baffled internal structures, and designs that have many mixing points. Lv et al. [4] used external AC electrodes at the bottom of the micromixer to improve the mixing performance by joule heating effect and the heat generated externally; the results showed that the mixing index was increased up to 83% and even exceeds 90% when a film heater was applied. However, there was a challenge of failing to rapidly cool the microreactor when the temperature reaches high levels. Lv et al. [5] also looked at the optimal design of the internal structures which is called the cantor fractal structure (baffles) which were added in the Y-shaped micromixer to improve the micromixing efficiency; the results of mixing performance showed tremendous improvement; however, there were increased pressure drops due to the baffle design. Another challenge reported by other researchers is channel blockage in baffle designs.

To achieve high mixing performance and to enhance the effects of convection on the mixing, channel geometries such as T and arrow micromixers have been investigated using Villermaux–Dushman protocol in terms of mixing efficiency achieved. The investigation showed that the corners or serpentine shapes achieve better mixing [6] 7. You et al. [2] numerically improved the outcomes of micromixers by varying the inlet angles of the micromixers. They came to the conclusion that the entry angle of micromixers into the main channel has a significant impact on mixing performance. The Y-shaped microreactor had a lower pressure drop as compared to other shapes of microreactors, also it has high mixing performance than other microreactors. More so, numerical simulations have been done to study the effect of geometrical parameters on micromixing efficiency and heat transfer. Therefore, it is crucial to develop efficient microreactors to increase the mixing efficiency for the development of microreaction systems.

Thus, in this work, a novel microreactor design has been developed to improve the micromixing efficiency and the mixing time. The novel design has a multistage Y-A shape as, according to literature, Y has better entry mixing efficiency of the feed streams. The geometry is designed in order to enhance the turbulence and vortices inside the microreactor. The novelty of the microreactor is on the unique shape of the two-stage combining and splitting streams and also 12 corners to improve the mixing of the fluids when they recombine. The effect of the Y angle on micromixing efficiency is also studied using 60° and 45° angles.

The microreactor is made of polymethyl methacrylate (PMMA) material which is a transparent material for easy visibility and light exposure. The conversion mixing and thermal mixing performance is characterized using the iodide/iodate chemical reaction (Villermaux–Dushman) and thermal camera. Segregation index analysis is also used to model the micromixing efficiency of the microreactors. And absorbance and reactant concentration were used to calculate the micromixing time. Additionally, the computational fluid dynamics (CFD) using Ansys software was performed to assess the mixing efficiencies of the multistage Y-A-shaped microreactor of different angle geometries [8]. The microreactors can be used in synthesis of pharmaceutical drugs or intermediates, polymers, wastewater treatment and nanoparticles [9].

2 Experimental methodology and protocol

2.1 Fabrication of microreactors

Figure 1 depicts the proposed microreactors, which were created through laser ablation with a laser cutter machine. Polymethyl methacrylate sheets were used to make the microreactors. The channel diameter was 500 microns. Two syringes of volume 12 ml each were used as feed for the chemicals. Small (milli)-sized pipes, epoxy and other accessories were used for the connection. The reason for choosing two stages after the Y shape was to have the splitting and recombining sections which give a lag in the mixing when the two split streams are recombining. This lag does not exist in the circle channels as the channel has no sharp edges, so the two split streams are recombining smoothly, resulting in better mixing, and also the shape of the stages was chosen to have 12 sharp corners which increase the turbulence and create more eddies in the fluid flow, thus aiding in micromixing efficiency [10].

2.2 Numerical simulation procedure

ANSYS-2022 software was used to simulate computational fluid dynamics in terms of vorticity, dynamic pressure and thermal mixing (wall temperature). The thermal mixing in ANSYS was compared with thermal mixing (wall temperature) done experimentally which was characterized by the thermal camera.

2.2.1 Governing equations and numerical methodology

Continuity, momentum and species transport equations of incompressible steady flows are presented by the following equations:

Continuity equation:

$$\nabla \vec{V} = 0 \tag{1}$$

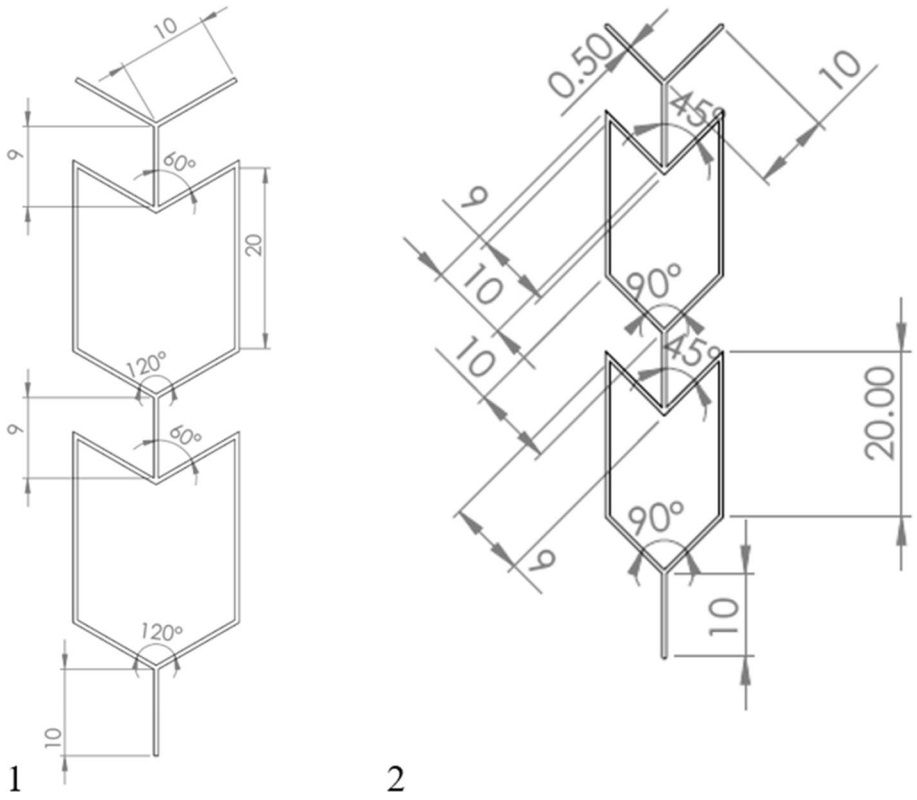

Fig. 1 The fabricated microreactor designs (1) 60° microchannel and (2) 45° microchannel

Momentum equation:

$$\left(\vec{V}\nabla\right)\vec{V} = -\frac{1}{\rho}\nabla P + \nu\nabla^2\vec{V} \tag{2}$$

where P, V and $'\rho$ present the static pressure, velocity and density of the fluid, respectively.

For Newtonian fluid flow, the species transport equation is expressed as follows [11];

$$\vec{V}\nabla = D\nabla^2 C_i \tag{3}$$

Uniform velocities were imposed at the inlets and different temperature (300 K and 328 K) with a no-slip boundary condition applied on the other parts of the walls and zero static pressure at the outlet section.

All governing equations in the proposed micromixers were solved in a laminar regime by using ANSYS flow simulation Fluent 2022 [12]. The computations were ensured and simulated to be converged at 10^{-6} of root mean square (RMS) residual values. Pure water liquids were used as a working fluid, with a fluid density of 1000 kg/m^3 and the diffusion coefficient equal to 1×10^{-11} m^2/s, in order to do comparison on outlet temperatures between two microreactor designs by varying inlet velocity of both inlet A and inlet B, corresponding to the flowrate values: 100 ml/h, 200 ml/h, 300 ml/h, 400 ml/h, 500 ml/h and 600 ml/h.

The Reynolds number is defined as follows:

$$\mathrm{Re} = \frac{\rho V D_\mathrm{h}}{\mu} \tag{4}$$

where D_h is the microchannel diameter and μ is the kinematic viscosity [13].

2.3 Numerical validation

A numerical steady state of mixing flows of water fluid inside the two microreactors was solved in order to validate computation fluid dynamic (CFD) accuracy.

2.4 Theoretical procedure

2.4.1 Villermaux–Dushman protoco/

The protocol to perform the Villermaux–Dushman reaction with the correct concentration sets is explained below:

In stage 1, to get the mixing time, firstly pressure drops of the microreactors are determined. Two pressure sensors are used to detect the pressure drop across the microreactor, one at the intake and the other at the outflow. While the streams that are running through the microchannels are passive, the

pressure drop is measured. A twin syringe pump is therefore employed, and both syringes are loaded with pure water. Since both inlets have the same geometry and flow rate, one pressure sensor is sufficient to monitor the pressure at a single intake. The two manufactured microreactors underwent this operation, and the pressure drops were calculated. The experiment was repeated 3 times for each flowrate for both microreactors.

Then the energy dissipation was calculated from the following correlation [15]:

$$\varepsilon = \frac{Q\Delta P}{\rho V} \tag{5}$$

where ε is the energy dissipation rate per unit mass (W/kg), Q is the flow rate through the microreactor (m^3/s), P is the pressure drop across the microreactor inlets and outlet while the flow is nonreactive (Pa), ρ is the density of the flowing fluid (kg/m^3) and V is the holdup volume of the microreactor (m^3).

Commenge and Falk [14] generalized data of 8 types of microreactors and came up with the conclusion that the mixing time is related to specific energy dissipation rate per unit mass ε according to the following relation [14, 16];

$$t_m = 0.15\,\varepsilon^{-0.45} \tag{6}$$

where t_m is the estimated mixing time (s) and ε is the energy dissipation rate per unit mass (W/kg).

In stage 2, after calculating the theoretical mixing, the correlation made by Commenge et al. 2011 is then used to determine the appropriate concentration sets to do the experiments. According to the correlation made by Commenge et al. [15], the concentration sets that can be used relating to the theoretical mixing time are concentration sets 1, 1c, and 2b from Table 1 were chosen to test for the mixing efficiency of the microreactors. Concentration sets 1 and 1c have identical buffered iodide/iodate solution concentrations, but the acid concentration is different. Concentration sets 1 and 2b, on the other hand, have equal sulfuric acid concentrations, whereas the buffered solutions differ. As a result, the solutions in concentration sets 1c and 2b are completely different. Two buffer solutions and two acid solutions are prepared for carrying out the Villermaux–Dushman reaction. The units for the concentration are (mol/L).

Table 1 Concentration sets used for the mixing performance test

Species	$[H^+]$	[KI]	$[KIO_3]$	[NaOH]	$[H_3BO_3]$
set 1	0.03	0.032	0.006	0.09	0.09
set 1c	0.04	0.032	0.006	0.09	0.09
set 2b	0.03	0.016	0.003	0.045	0.045

2.5 Micromixing characterization

By conducting the iodide/iodate reaction (Villermaux–Dushman reaction) within the microchannels, whose process is as follows, the mixing efficiency within each microreactor is examined [16, 17].

$$H_2BO_3^- + H^+ \leftrightarrow H_3BO_3$$

$$IO_3 - +5I - +6H + \ \leftrightarrow 3I_2 + 3H_2O$$

According to this mechanism, the Villermaux–Dushman reaction is a competing reaction composed of a neutralization reaction (the first reaction) and a redox reaction (the second reaction).

The redox reaction is faster than the micromixing process but much slower than the neutralization reaction.

In a perfect ideal situation, the acid is solely used up in the neutralization process, and the protons' (H+) stoichiometry defect prevents the redox reaction from happening [18]. Acid takes a long time to dissipate if mixing is poor, taking much longer than the typical redox reaction time. The acid remains once all of the borate ions have been consumed. It combines with iodide (I^-) and iodate (IO_3^-) ions to produce iodine (I_2). The amount of generated iodine (I_2) reveals the fluid's segregation status and it indicates yield. Then, based on quasi-instantaneous equilibrium, triiodide is generated via the reaction between the produced iodine (I_2) and iodide ion (I^-),

$$I_2 + I- \leftrightarrow I_3^-$$

Kc the equilibrium constant is a function of temperature and is calculated with the following relation

$$\log_{10} K_C = \frac{555}{T} + 7.355 - 2.575 \times \log_{10} T \tag{7}$$

$$K_C = \frac{[I_3^-]}{[I_2] \times [I^-]} \tag{8}$$

The concentration of triiodide produced by the quasi-instantaneous equilibrium reaction is the only measure of the mixing efficiency whether it is good or poor mixing [7]. The concentration of triiodide formed can be obtained from the Beer lambert law;

$$[I_3^-] = \frac{A}{\varepsilon_{353} \times l} \tag{9}$$

where ε_{353} is the molar extinction coefficient at a wave length of 353 nm which was 26 047 L/mol.cm, l is the optical path length of the spectroscopic cell = 1 cm and A is the absorbance.

The segregation index Xs and the micromixedness ratio can be computed using the UV spectrophotometry results.

These characteristics were fully detailed as follows by Guichardon and Falk [19]:

$$X_s = \frac{Y}{Y_{cs}} \tag{10}$$

where Y is the ratio of the acid consumed by the second reaction to the total amount of acid fed to the system. Y_{CS} is the value for complete segregation [20]. For a mixer with the same flowrate for both solutions, the equations for Y_{CS} and Y are

$$Y = \frac{4 \times \left(\left[I_2 \right] + \left[I_3^- \right] \right)}{\left[H_{,0}^+ \right]} \tag{11}$$

$$Y_{CS} = \frac{6 \times \left[IO_{3,0}^- \right]}{\left(6 \times \left[IO_{3,0}^- \right] \right) + \left[H_2BO_{3,0}^- \right]} \tag{12}$$

where subscript 0 denotes the inlet concentrations of the component in the respective solutions.

The micromixedness ratio ά is the ratio of the perfectly mixed volume V_{PM} to the totally segregated volume V_{cs}:

$$\propto = \frac{V_{PM}}{V_{cs}} \tag{13}$$

$$\propto = \frac{1 - X_S}{X_S} \tag{14}$$

2.6 Experimental procedure

2.6.1 Equipment and chemicals

Double-syringe pump (115 VAC Cole-Parmer™, USA), Kobold pressure measuring device (HND-P215) with 2 external sensors (HND-PS19), HITACHI UV Spectrophotometer (U-3900) equipped with cuvettes of 1 cm optical path length, and FLIR T865 Thermal camera were accessed from different laboratories in E-JUST. The chemicals include potassium iodate (Rankem™, RFCL Limited, India), the hydrochloric acid of 37% purity (Fisher Scientific, UK), sodium hydroxide pellets (AppliChem GmbH, Germany), boric acid (MP Biomedicals, LLC, France), and 99% pure potassium iodide (Chem-Lab NV, Belgium), which were all analytical grade and were obtained at E-JUST under the Chemical and Petrochemicals Engineering department.

2.6.2 Acid solution preparation

The concentration of the acid solution for sets 1 and 2b is 0.03 mol/L. The concentration of the acid solution for set 1c is 0.04 mol/L. The acid solution was prepared by diluting concentrated HCl from a stock solution of approximately 37% with a density of 1.2 g/ml. Hence, to prepare 0.03 mol/L HCI solution, 1.25 mL of concentrated HCl was diluted in distilled water up to 500 ml and it was labeled acid solution set 1 and 2b. To prepare 0.04 mol/L HCI solution, 1.64 mL of concentrated HCl was diluted in distilled water up to 500 ml and it was labeled acid solution set 1c. It should be noted that acid was added to the distilled water but not the other way round, for safety reasons.

2.6.3 Buffer solution preparation

The buffer solution for sets 1 and 1c was prepared by first forming an aqueous NaOH solution by weighing 1.8 g of NaOH pellets and dissolving it in 80 ml of distilled water. Then, 0.64, 2.65, and 2.78 g of KIO_3, KI, and H_3BO_3, respectively, were weighed and dissolved in the aqueous NaOH solution and the mixture was made up to 500 mL and labeled buffer solution set 1 and 1c.

The buffer solution for set 2b was prepared by first forming an aqueous NaOH solution by weighing 0.09 g of NaOH pellets and dissolving it in 80 ml of distilled water. Then, 0.32, 1.235, and 1.39 g of KIO_3, KI, and H_3BO_3 respectively, were weighed and dissolved in the aqueous NaOH solution and the mixture was made up to 500 mL and labeled buffer solution set 2b (Fig. 2).

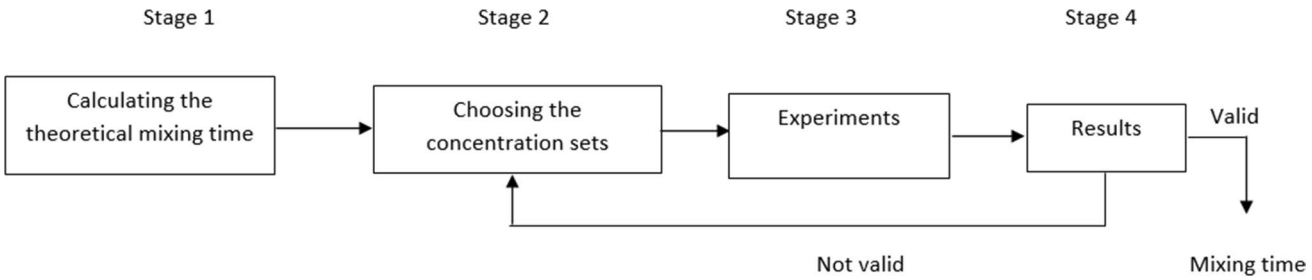

Fig. 2 Recommended steps for the Villermaux–Dushman system to characterize micromixers [14]

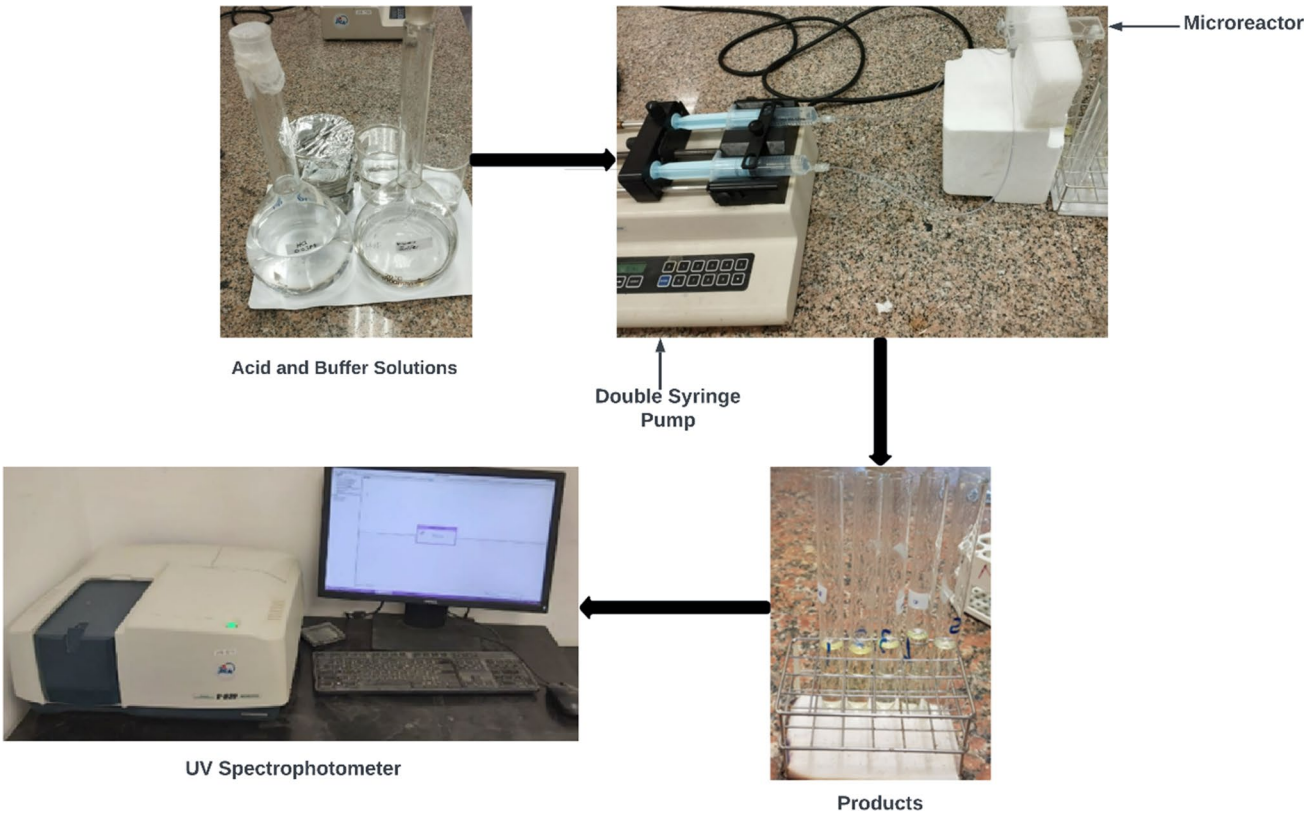

Fig. 3 Schematic diagram of the micromixing test system

In Stage 3, Villermaux–Dushman reaction, the experimental setup was created as depicted in Fig. 3 to carry out the Villermaux–Dushman reaction in the manufactured microreactors. It used a syringe pump with two syringes, each with a diameter of 27.54 mm and a capacity of 12 ml. The two syringes were filled with distilled water before the reaction began, and the microreactor's microchannels were rinsed with the syringe pump while it is operating at a moderate flow rate. Then, 12 mL of the acidic solution was placed in syringe 1 and 12 mL of the buffer solution is placed in syringe 2. The microreactor's first 4 mL downstream was discarded as garbage. The sample was then removed to be evaluated using the UV spectrophotometer. In each microreactor, the reaction was run six times at various flow rates of 100 mL/h, 200 mL/h, 300 mL/h, 400 mL/h, 500 mL/h, and 600 ml/h to examine the impact of the flow regime on the mixing of the reactants in the microchannels. The experiment was repeated for all the 3 concentration sets.

In Stage 4, Results collection, the two microreactors were operated at different flow rates, so per every flow rate and concentration set, 3 samples for each microreactor were examined for the concentration of triiodide and the average of the three was taken as the absorbance. All samples were measured at a wavelength of 353 nm since it has a strong affinity for the UV spectrum. All samples were compared to distilled water as the standard. Then, the absorbance of each sample is determined in relation to distilled water. The optical path of the quartz cuvettes utilized inside the UV spectrophotometer is 10 mm. After every measurement, the cuvette was cleaned with distilled water to make sure it wasn't contaminated by the sample before.

2.6.4 Batch system

In the batch system, the Villermaux–Dushman reaction was also performed by mixing 10 mL of the acidic solution with 10 mL of the buffer solution. The two solutions were then batch-mixed together. To compare the reactor performance and mixing efficiency between the microreactor system and the batch system, the products were analyzed using a UV spectrophotometer.

2.6.5 Thermal mixing experiment

Water was used as the fluid, inlet A was maintained at 55 °C and inlet B was maintained at 27 °C. A thermal camera was used to analyze the temperature inside the microreactor as the hot and cold streams were mixing. The outlet temperature was measured using a temperature meter and the results

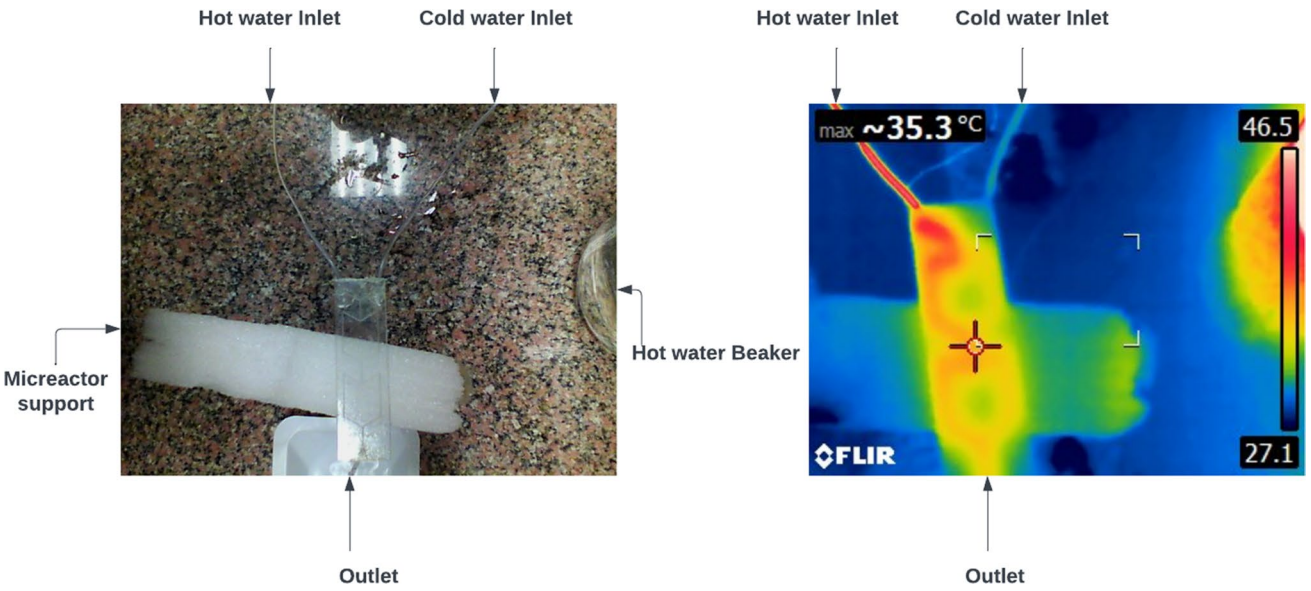

Fig. 4 Thermal photograph

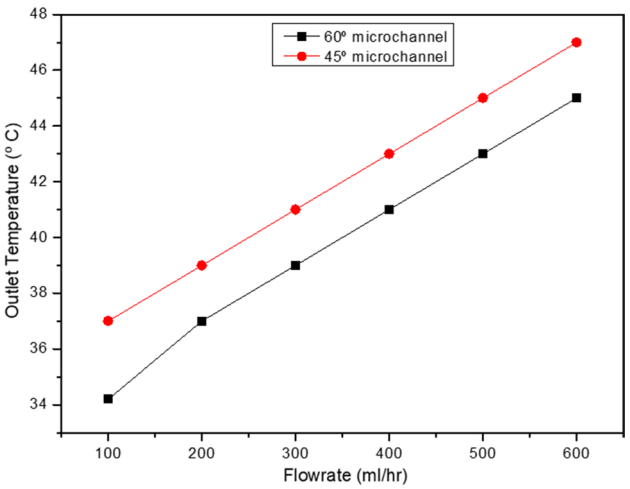

Fig. 5 Effect on outlet temperature

were recorded. This experiment was repeated for both the microreactors at 6 different flow rates. As shown in Fig. 4, the hot stream is redder and the cold stream is a bit yellow (Figs. 5, 6, and 7).

3 Results and discussion

3.1 Simulations on thermal mixing

3.1.1 Effect of flowrate on outlet temperature

Figure 8 confirms that most microreactor shows higher dynamic pressure drop due to lower channel diameters [21]. The simulations show that the 45° angle microreactor has a high dynamic pressure drop because of the very sharp corner, which causes flow delays. However, the sharp corner gives higher vorticity as seen in Fig. 7. From simulation results, we can see that the 45° angle microreactor had better thermal mixing than the 60° angle microreactor. And these results are consistent with the experimental results but with few deviations which could be results of meshing, the roughness of actual models, and the deviation of dimensions of the actual model [22].

3.2 Determining the theoretical mixing time

3.2.1 Effect of flowrate of pressure drop

Figure 9 shows that the pressure drop is directly proportional to the flow rate of the inlet streams of the microreactor. The pressure drop of the 45º microreactor increases at a constant rate, while the pressure drop of the 60º microreactor increases fast from 100 up to 500 ml/min then after 500 ml/min the rate of increase reduces. This means that as the flowrate is continued to increase, its effect on pressure starts to be insignificant for the 60º microchannel. The 60° channel has the lowest pressure drop compared to the 45°. The design of the microreactor generally induced pressure drop due to the splitting and recombination of fluid streams [23]. The 45° channel microreactor had larger pressure drops which were attributed to the steepness of the angle and channel as compared to 60°.

For both the two types of channels, they had two splitting and two recombining sections, so the flow is not flowing smoothly as the flow through the straight channel. More so,

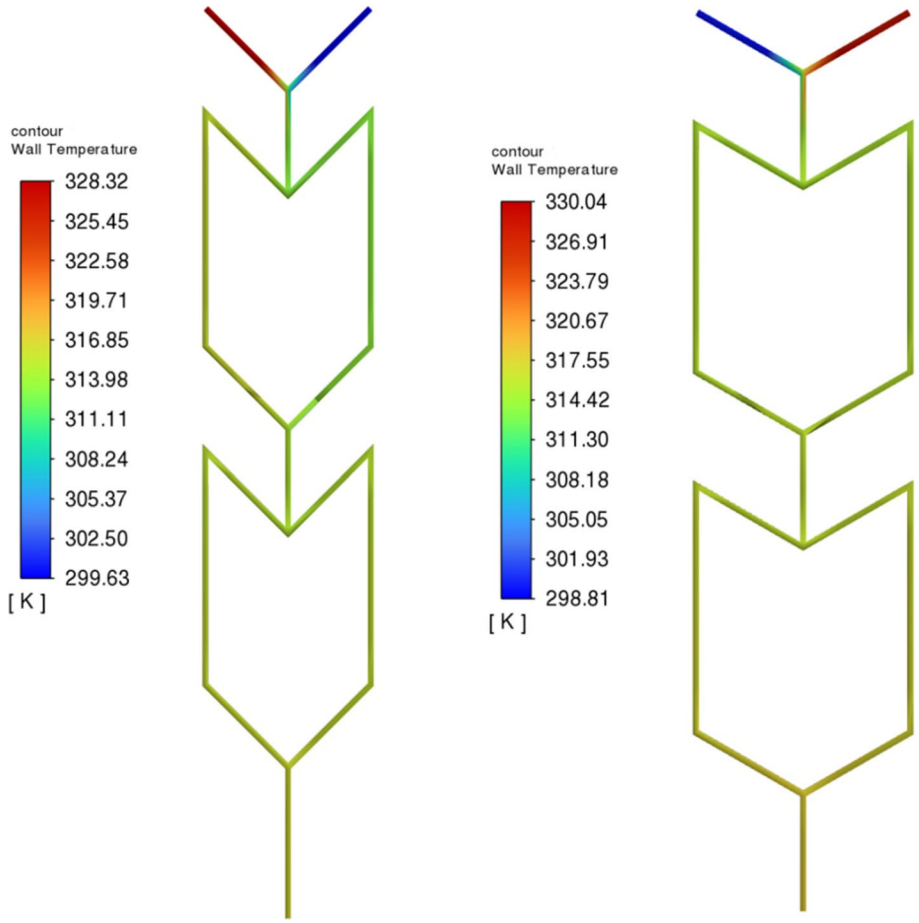

Fig. 6 Wall temperature contours for 45° and 60° microchannels

both the microreactors have twelve sharp corners at which the flow hits, so the flow pressure decreases due to these corners [10]. The 45° and 60° channels have a repeating sequence of Y shapes that lowers the pressure of the flow streams throughout the channels.

3.2.2 Energy dissipation rate

The energy dissipation rate per unit mass is calculated from the equation below based on the measured pressure drops above

$$\varepsilon = \frac{Q\Delta P}{\rho V} \tag{15}$$

The energy dissipation rate per unit mass of the 45° microchannel was higher than that of 60° due to the higher pressure drops in the former channel than in the later. Since pressure drop increased with an increase flow rate, energy in-turn increased with an increase in flowrate since it is directly proportional to the pressure drop. The energy dissipation rate per unit mass increases very fast at the first and then after 500 ml/min; its rate of increase declines, as seen by the deviation increase between the 2 graphs when flowrate reaches 500 ml/min and above. This is so since at higher flowrate the effect of flowrate on pressure drop begins to reduce, thus affecting the energy dissipation rate per unit time. The calculated energies are in agreement (same range) with the values calculated by Kolbl et al. (2008) which comprised between 0.1 and 40 W/kg for a flowrate range of 10–400 ml/h for a V-type microreactor.

3.2.3 Theoretical mixing time

The following mixing time was based on the relation with the calculated energy dissipation rate per kg using the following equation

$$t_{\mathrm{m}} = 0.15\varepsilon^{-0.45} \tag{16}$$

The theoretical mixing time enables us to choose a set of concentration sets to use for the Villermaux–Dushman protocol [24]. From the graph, it can be seen that the theoretical mixing time for the 45° channel was smaller as compared to

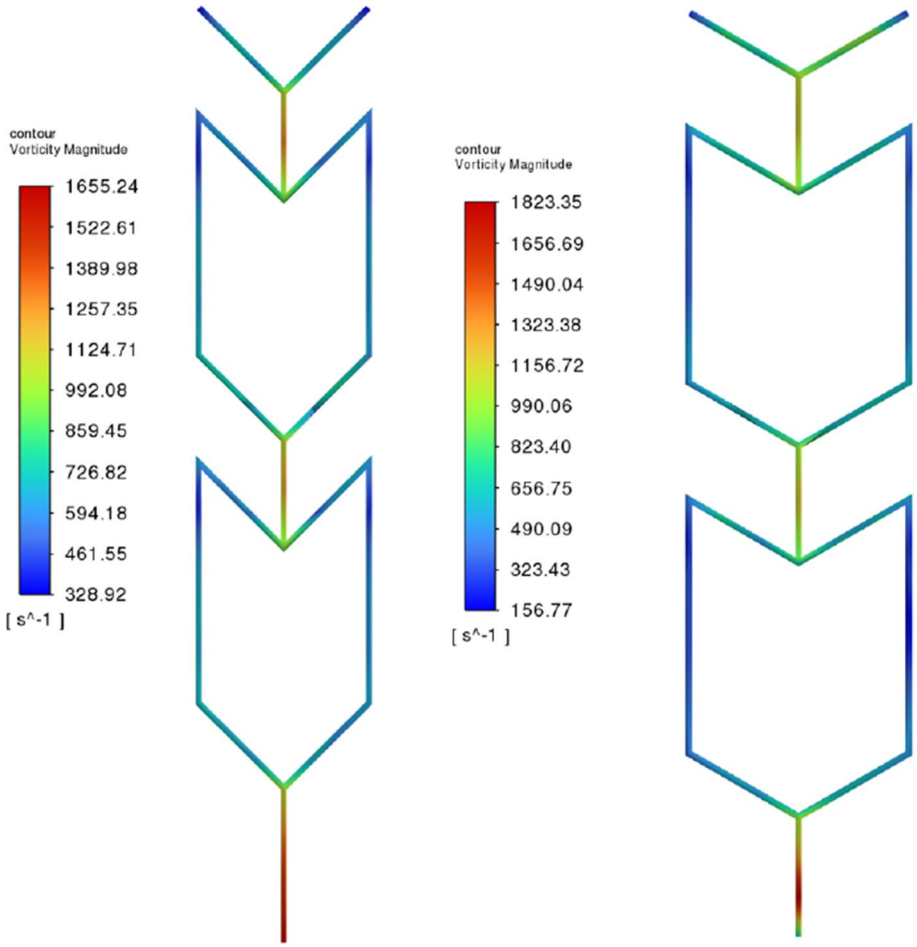

Fig. 7 Vorticity contours for 45° and 60° microchannels

the 60° channel due to the higher energy dissipated in the 45° channel than in the 60° channel. The theoretical mixing time drops very fast as soon as the flowrate is increased, and then from 300 ml/min going forward, the effect of increasing flowrate on theoretical mixing time actually becomes negligible since at higher flowrates, pressure drop increase starts to reduce. As the flowrate increases, the energy dissipation rate per unit mass increased due to high-pressure drop, thus resulting in a higher theoretical mixing time [25]. After obtaining the estimated mixing time, it enables the creation of an operating window from which the appropriate concentration sets can be selected (step 2 in Fig. 2) [26]. This operating window contains three possible concentration sets: 1, 2b, and 1c. The differences between these concentration sets should be highlighted before analyzing the results. Concentration sets 1 and 1c have identical buffered iodide/iodate solution concentrations, but the acid concentration is different. Concentration sets 1 and 2b, on the other hand, have equal sulfuric acid concentrations, whereas the buffered solutions differ. As a result, the solutions in concentration sets 1c and 2b are completely different [27] (Figs. 10 and 11).

3.3 Experimental results of mixing efficiency.

3.3.1 Effect of flowrate and concentration sets on the UV absorbance

Figures 12 and 13 show the effect of flowrate and different concentration sets on absorbance. The UV absorbance test, which indicates the concentration of the formed triiodide, is used to investigate mixing efficiency. Triiodide absorbs the ultraviolet ray at 353 nm with a high affinity. Because perfect mixing occurs when triiodide is not formed and all hydrogen ions are consumed by the neutralization reaction rather than the redox reaction, the higher the concentration of triiodide, the higher the absorbance value, and the less efficient mixing [28].

Experiment results show that increasing the flow rate improves mixing efficiency as the concentration of triiodide decreases with decreasing measured absorbance. When flow rates increase, molecules collide much more with each other due to the formation of eddies in the flowing stream, which improves mixing.

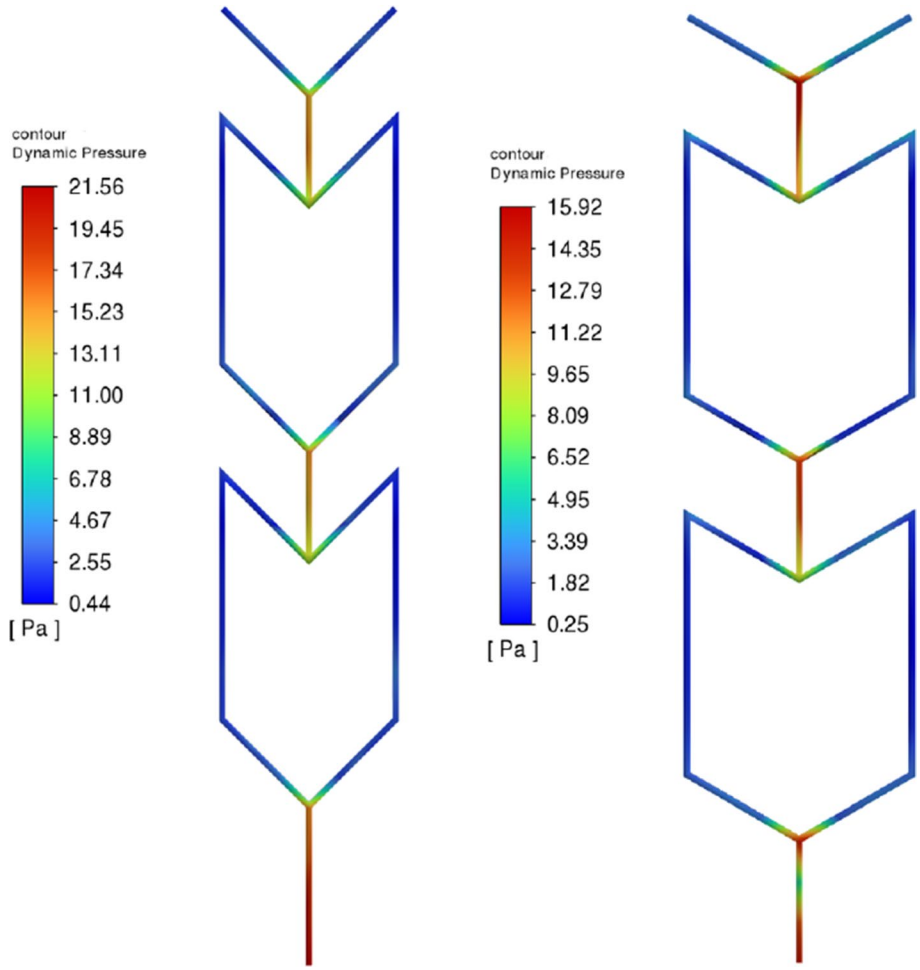

Fig. 8 Dynamic pressure for 45° and 60° microchannels

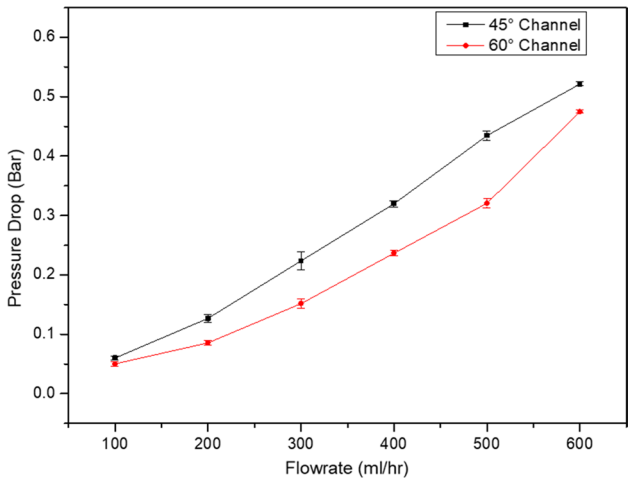

Fig. 9 Effect of flowrate on pressure drop

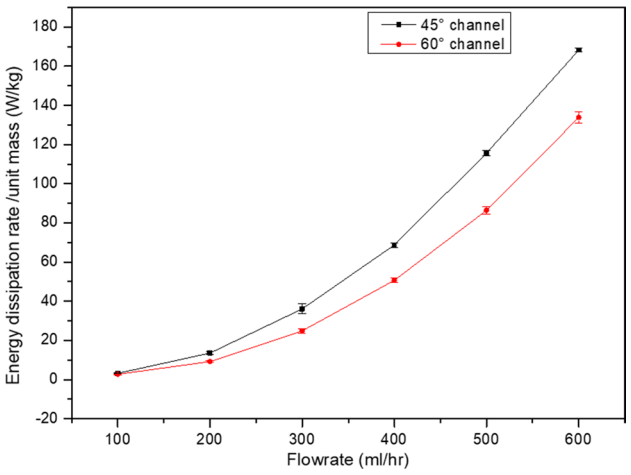

Fig. 10 Effect of flowrate on energy dissipation rate per unit mass

The absorbances measured with concentration sets 1 and 2b precisely overlap, as expected given their similar characteristic curves by Commenge et al. [17]. Concentration set 1c, as expected from the same figure, provides higher absorbance for equal flow rates, corresponding to shorter mixing times. The absorbance determined by set 1c is of greater magnitude. The explanation is that the characteristic reaction time for set 1c is significantly shorter due to the

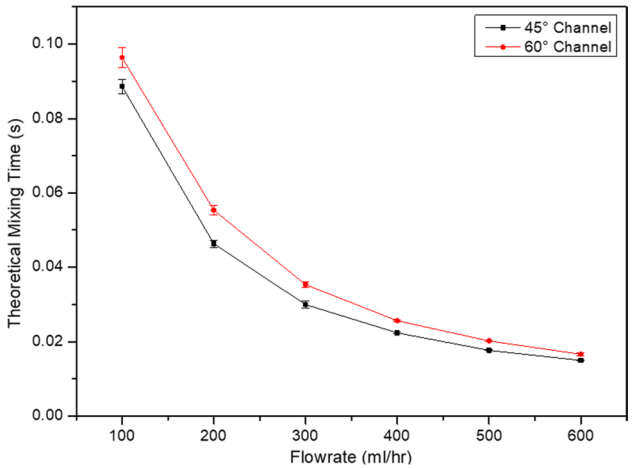

Fig. 11 Theoretical mixing time vs flowrate

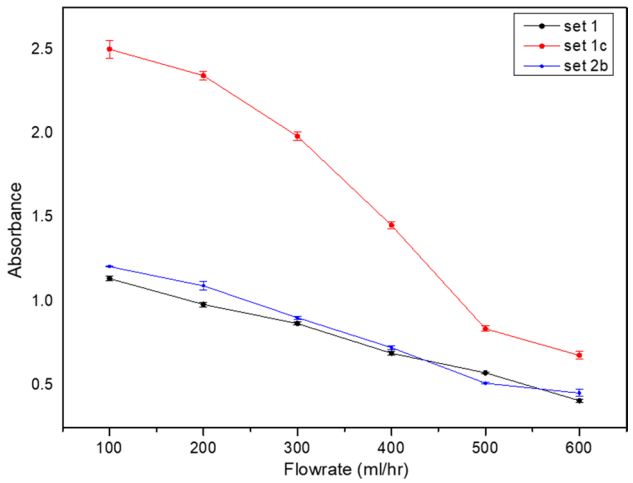

Fig. 12 Effect flowrate and concentration sets on UV absorbance (60° microchannel)

higher acid concentration. As the flowrate is just increased, the absorbance values of set 1c decrease sharply, and as the flowrate reaches 500 ml/min, the rate of decreases reduces; for all the 3 concentration sets, this shows that further increase in the flowrate has little effect on the reaction efficiency, for the 2 microreactors as seen by the intertwining absorbance values for set 1 and 2b at higher flowrates. At constant mixing times, the mixing time-to-reaction time ratio is greater, resulting in increased iodine and triiodide formation in both microreactors.

From the obtained results, it is shown that the 60° channel has the lowest mixing efficiency as it has slightly higher values of absorbance at all the studied flow rates as compared to the 45° channel. Generally, both the microreactors had good micromixing due to the splitting and recombining

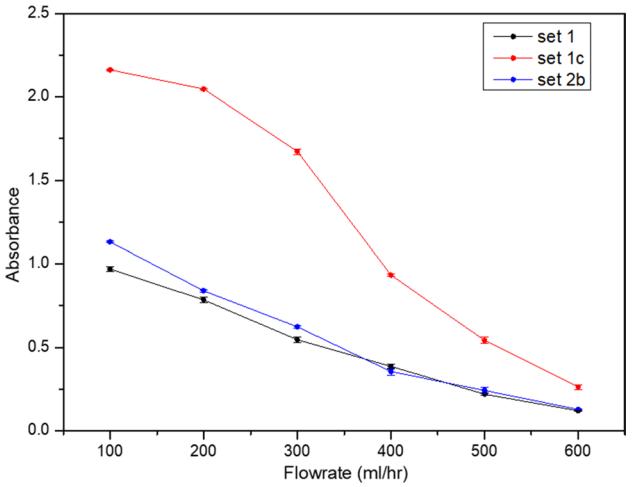

Fig. 13 Effect of flowrate and concentration sets on UV absorbance (45° microchannel)

sections that are involved in the channel designs and also 12 sharp corners which increased the turbulence in the fluid flow, thus aiding in micromixing efficiency, so they have fewer absorbance values as compared to the other designs studied in the literature [21]. However, the 45° channel has better mixing performance than the 60° at all of the studied flow rates and concentration sets because of the sharper corners created by the 45° channel which create more eddies than the corners in the 60° channel. Therefore, there is a lag in the mixing when the two split streams are recombining. This lag does not exist in the circles channel as the channel has no sharp edges, so the two split streams are recombining smoothly, resulting in better mixing [29].

3.3.2 Experimental mixing time

The mixing time was calculated from the absorbance using the following equation [20].

$$t_m = 0.33(\mathrm{OD})\left[H^+\right]^{-4.55}[\mathrm{KI}]^{-1.5}[\mathrm{KIO3}]^{5.8}[\mathrm{NaOH}]^{-2}\left[H_3BO_3\right]^{-2} \quad (17)$$

The mixing time of 2b and 1 is slightly close together as expected from the correlation by Commenge [15], and the mixing time from set 2b is slightly lower than that of set 1. Set 1c has the lowest mixing time for both reactors as expected from the correlation by Commenge [15]. The 45° microreactor had a lower mixing time which attributed to better mixing performance as compared to the other reactor. The higher the flow rate, the shorter the mixing time leading to better mixing performance for both the microreactors. While the concentration sets differ (and sometimes yielded different absorbances), all of the experimental data

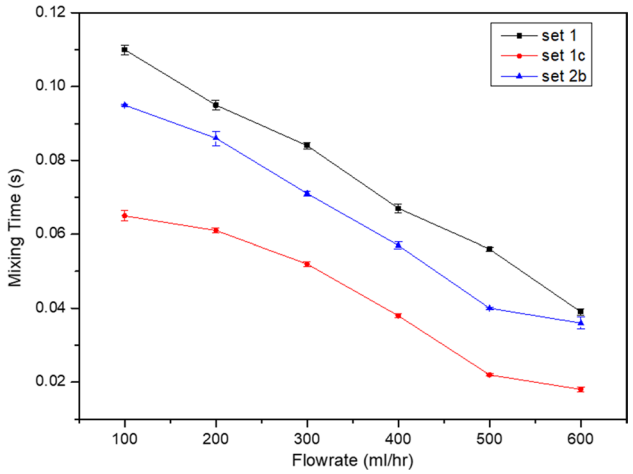

Fig. 14 Effect of flowrate and concentration sets on experimental mixing time (60° microchannel)

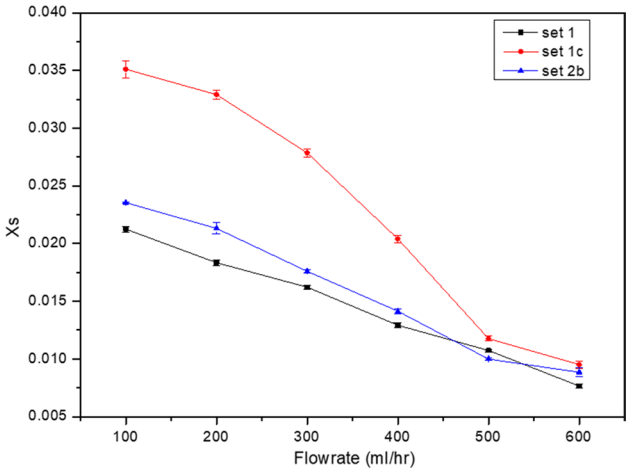

Fig. 16 Effect of concentration sets and flowrate on segregation index (60° microchannel)

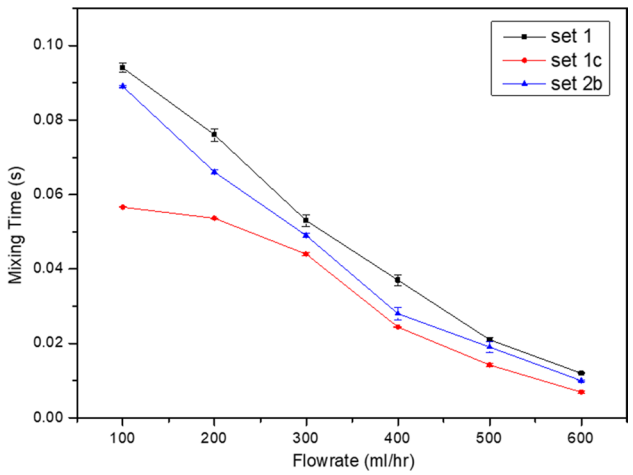

Fig. 15 Effect of flowrate and concentration sets on experimental mixing time (45° microchannel)

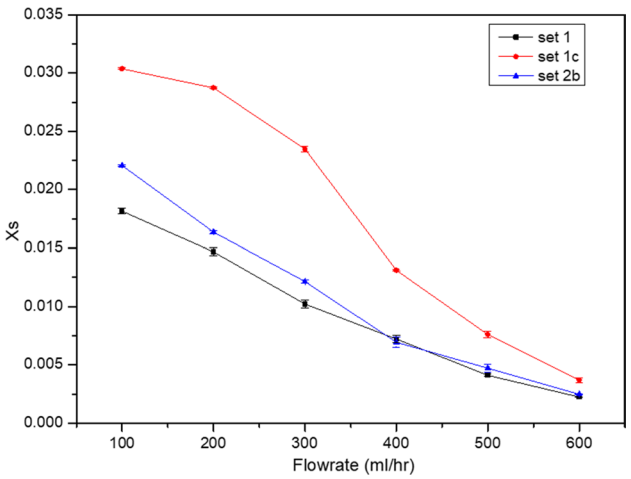

Fig. 17 Effect of concentration sets and flowrate on segregation index (45° microchannel)

converted to mixing times form a single curve, the trend, and magnitude of which are consistent with values from the literature compared by (Falk and Commenge et al., 2011) and preliminary estimates from pressure drop calculations (step 4 in Fig. 2). This finding provides experimental evidence that the Villermaux–Dushman protocol is a reactant concentration-free method for mixing quantification [21]. For both the microreactors, the mixing time for concentration set 1c is negligibly affected by an increase in flowrate until the flowrate reaches around 300 ml/hr. where the decline in mixing time is very sharp. But, however, for sets 1 and 2b, the rate decrease is constant with an increase in Reynolds number for both the microreactors (Figs. 14 and 15).

3.3.3 Segregation index and micromixedness ratio

Figures 16 and 17 show the segregation index vs the flow rate. Analysis of the mixing performance using the segregation index gives a better outlook of how the microreactors performed. Set 1 had the lowest segregation index followed by set 2b and lastly set 1c. As the flowrate increased, the segregation index decreased for both the 2 microreactors and the 3 concentration sets. There is a drastic decline in the segregation index for both the microreactors up to 400 ml/min, and as the flowrate is increased from this, the change is minimal, the rate of decrease becomes negligible as seen by the almost the same intermixed Xs values for set 1 and 2b at higher flowrates and the reduced Xs difference between the set 1c and the other 2 sets at a flowrate of 600 ml/min. The

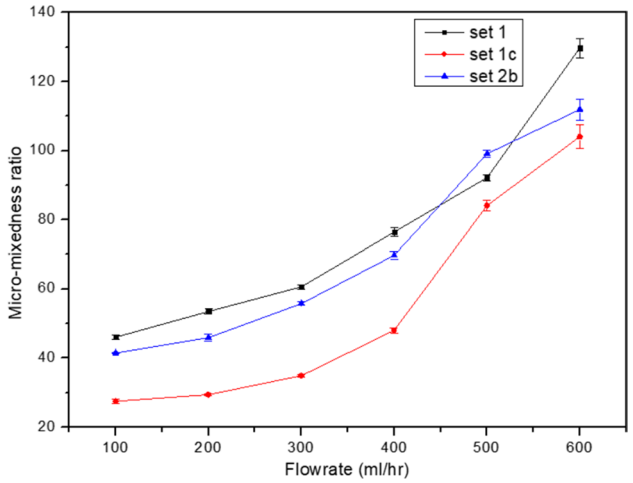

Fig. 18 Effect of flowrate and concentration sets on $\acute{\alpha}$ (60° microchannel)

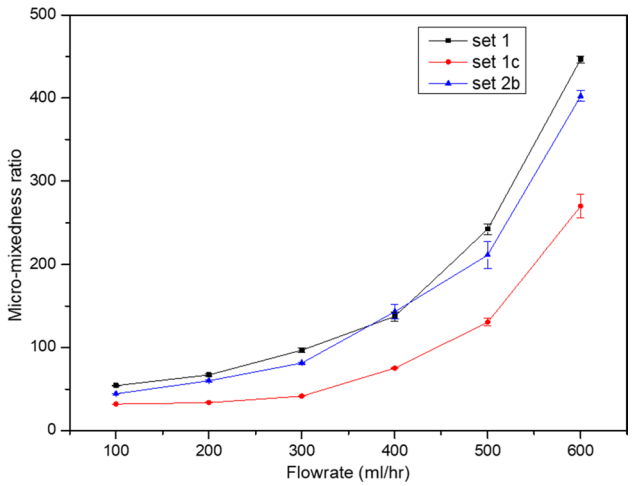

Fig. 19 Effect of flowrate and concentration sets on $\acute{\alpha}$ (45° microchannel)

effect of the change in flowrate on segregation index reduces at higher flowrates. This is so because the vast amount of H^+ reacts with $H_2BO_3^-$ [24]. High flowrates promote local turbulences in the reaction matrix and in the microreactor corners, thus promoting efficient micromixing, meaning the first reactions happens more efficiently reducing the production of unwanted triiodide [12] (Figs. 18 and 19).

Xs is high for set 1c, due to the higher acid concentration as compared to the other microreactors, which could be attributed to the very fast side reaction (iodine formation) in presence of more H+. With increase in acid concentration, more iodine is produced which contributes to increasing the segregation index [30]. Generally, both the microreactors had very good mixing as the highest segregation index was at 0.035102 which considerably very low according to literature. Due to the sharper corners in the 45° microchannel, there was more turbulence and eddies which aid in the micromixing efficiency than in the 60° microchannel [10].

3.3.4 Micromixedness ratio

The micromixedness ratio $\acute{\alpha}$ is the ratio of the perfectly mixed volume V_{PM} to the totally segregated volume V_{cs}:

$$\propto = \frac{V_{PM}}{V_{cs}} \tag{18}$$

$$\propto = \frac{1 - X_S}{X_S} \tag{19}$$

The higher the micromixedness ratio, the better the mixing. As the flowrate of reactants increased, the $\acute{\alpha}$ increased. The higher the value means the totally segregated volume is very low since total segregation means that there is imperfect mixing. The graphs shows that the 45° channel had higher micromixedness ratio than the other reactor due to the reasons explained in the effect of flowrate on absorbance. Set 1c had lower micromixedness ratio due to the larger UV absorbance which was attributed to the higher concentration of the H^+ acid in the reactants which results in more triiodide being formed. For both the microreactors, the micromixedness ratio slowly increases with an increase in flowrate on all the 3 concentration sets, but after 400 ml/min the change is rapid and sharp, showing that further increase in flowrate greatly affects the micromixedness ratio.

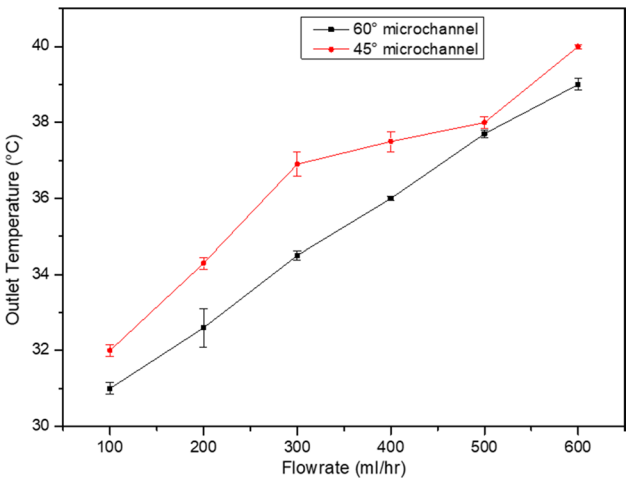

Fig. 20 Effect of flowrate on the outlet temperature

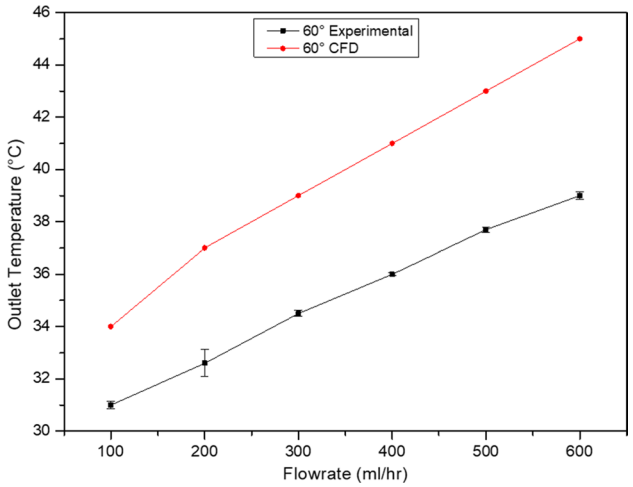

Fig. 21 Comparison of outlet temperature for CFD and experimental work (60° microchannel)

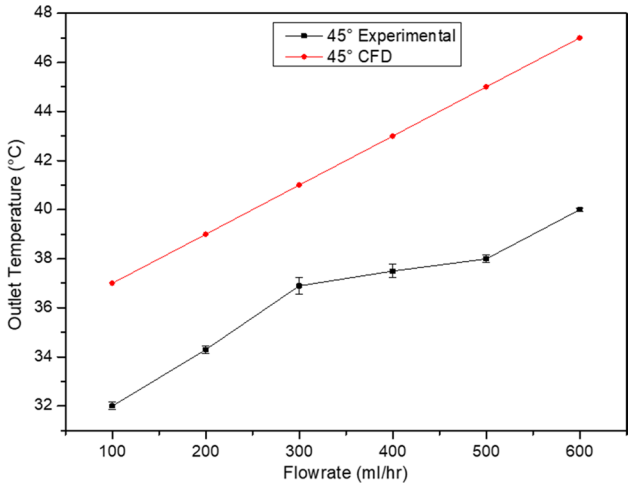

Fig. 22 Comparison of outlet temperature for CFD and experimental work (45° microchannel)

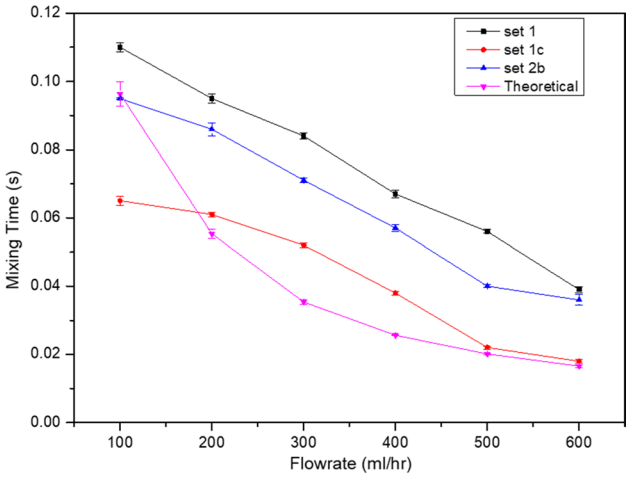

Fig. 23 Comparison of theoretical mixing time and experimental mixing time (60° microchannel)

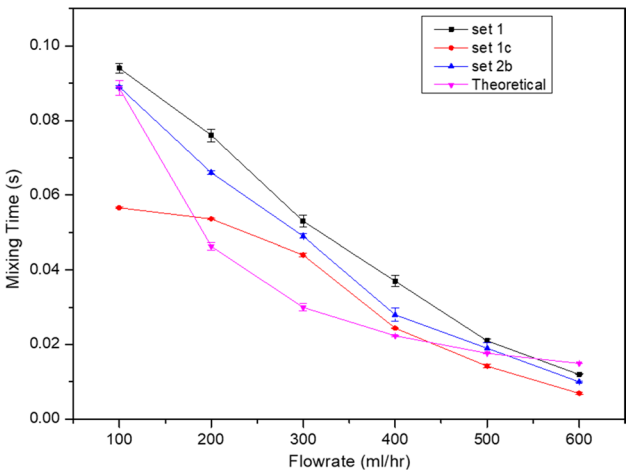

Fig. 24 Comparison of theoretical mixing time and experimental mixing time (45° microchannel)

3.3.5 Thermal mixing

The inlet temperatures were maintained at 55 and 27 °C.

Figure 20 shows the outlet temperature increased with an increase in flow rate. The 45° microreactor had a higher outlet water temperature on all the flowrate. The outlet temperature is always relative to the goal we want to achieve. If cooling the hot stream was the ultimate goal, then the 60° microreactor had better performance than the other reactor. However, if heating the cold stream was the ultimate goal, then the 45° microchannel had better output results. For the 45° microreactor, the outlet temperature increases steeply as the flowrate is increased, and the rate of increase reduces as the Reynolds number is further increased, whereas for the 60° microchannel, the rate of increase of outlet temperature is constant.

3.4 Comparison of simulation outlet temperature and experiment outlet temperature results

The simulation outlet temperature results are consistent with experimental outlet temperature results as seen in Figs. 21 and 22; as explained earlier the deviations occurred to meshing, the roughness of actual models; in actual experiment there are heat losses due to conduction and radiations [31].

Table 2 Micromixing time comparison of different microchannels

Channel shape	Technology of fabrication	Type of sample	Flowrate (ml/min)	mixing efficiency Xs = Segregation index Abs= absorbance	Surface modification	Mixing time ($t_{m)}$ (ms)	Advantages	Disadvantages	References
Zig-zag	Micromachining	H + = 0.03	1–8	3^{abs}	Two flat constructal distributors with bifurcation	9–44	High mixing performance due to higher Reynolds numbers arising from the fluid good mixing due to redistribution effect of the constructal distributors and bifurcation configurations	Channel blockage and high-pressure drop	[33]
Jet-shaped	Laser machining	H + = 0.16	10–50	$\approx 0.003^{Xs}$	none	3–60	Had a lower segregation index meaning higher mixing performance	High-pressure drop at a confluence angle	[12]
T-shaped	steel machining	H + = 0.05	4.8–40	0.002^{Xs}	42 kHz piezoelectric transducer, (ultrasound wave for sonication)	0.78–8.9	Ultrasound improved mixing performance (Active mixing) Can withstand high pressure	The sound produces local overheating which could affect some heat-sensitive products Hard to fabricate	[34]
Pore array (PA-TMCR)	laser machining	H + = 0.06	400–4500	$\approx 0.012^{Xs}$	Intensified tube-in-tube pore array	0.06–0.27	Pore array increased mixing performance	High-pressure drop at a higher annular size of 0.5 m	[35]
ZY-shaped SY-shaped ZDT-shaped	Additive manufacturing Additive manufacturing Additive Manufacturing	H + = 0.0026 H + = 0.0026 H + = 0.0026	64–160 64–160 64–160	0.77^{abs} 0.86^{abs} 0.733^{abs}	none	4.9–12.3 8.8–22.1 6.6–16.6	Efficient heat dissipation, high mass transfers, and short diffusion distance	Takes time to manufacture the microreactor Limited length and diameter of fabrication increase in pressure drop	[36]

Table 2 (continued)

Channel shape	Technology of fabrication	Type of sample	Flowrate (ml/min)	mixing efficiency Xs = Segregation index Abs= absorbance	Surface modification	Mixing time ($t_{m)}$ (ms)	Advantages	Disadvantages	References
Caterpillar variable-shaped	laser machining	$H+ = 0.0026$	1–18	≈0.001	Internal Structured caterpillar	2–12	High mixing performance due to internal structures of different shapes	Very high-pressure drop resulting in high energy input Complicated and expensive to manufacture	[37]
SAR with double-layer Y-shaped	CNC machining	Aqueous fluid in COMSOL = 0 and 1 mol/L	0.00675- 1.35	0.0008^{Xs}	none	none	Very high numerical and experimental mixing due to chaotic convection Smaller pressure losses	Expensive mode of fabrication Takes long procedure and time to clean	[32]
Multistage Y-A-shaped	Laser machining	$H^+ = 0.03$	1.6–10	0.1194^{abs} 0.002234^{Xs}	none	6.7–56.6	Cheap and easy to fabricate Good mixing even without external agitation passive mixer) Very high mixing even at low flowrates No channel blockages regardless of many corners Can be used in photocatalysis since its transparent	Pressure drop in the 45° microreactor	This work

3.5 Comparison of theoretical mixing time and experimental mixing time

The theoretical mixing time enables us to choose a set of concentration sets to use for the Villermaux–Dushman protocol [24]. From the graph, it can be seen that the theoretical mixing time for the 45° channel was smaller as compared to the 60° channel due to the higher energy dissipated in the 45° channel than in the 60° channel. From Figs. 23 and 24, converting the experimental values into mixing times according to Eq. 16 gives a magnitude and trend which is highly coherent and agreeing with the theoretical mixing time and values in literature [24], and also with the initial pressure drop calculations done (step 4 in Fig. 2). This finding serves as an experimental confirmation that the Villermaux–Dushman methodology is a non-concentration-dependent method for quantifying reactant mixing [24]. As explained earlier, the theoretical mixing time decreases steeply at the beginning and as flowrate continues to increase, its rate of decrease starts to reduce; as this value is pressure drop dependent, pressure drop increases and starts to reduce at higher flowrates.

3.6 Comparison of different microreactors

Table 1 shows the comparison of different microchannels with the present study. Absorbance (abs) and segregation index (Xs) were used as a comparison for the mixing performance depending on the parameters studied by the previous authors. It was observed that the multistage Y-A microchannel had better performance in terms of mixing efficiency and low-pressure drop as compared to other microchannels. This work demonstrated good mixing even at high Villermaux–Dushman concentrations of the buffer and acid, showing that the microreactor can be applied in different applications like pharmaceutical, wastewater treatment, etc. This work is contributing to the SAR with double-layer Y-shaped work in the sense that it's a simple design that does not require a complicated fabrication method or cleaning mechanism and it has minimum clogging as the channel is simple. This work had a high experimental mixing performance (Segregation index of 0.002234) which is quite close to the SAR microreactor numerical mixing performance of 0.9992 (Segregation index of 0.0008) [32]. The other contribution is that the current work investigated both the experimental and numerical thermal mixing performance of the microreactors and the good results showed that the design can be applied in heat transfer processes at minimal heat losses.

4 Conclusion

This work introduces the use of novel microreactor design of multistage Y-A shape with 2 varied angles 45º and 60º and its mixing performance in terms of Villermaux–Dushman reactions. The paper also looks at the comparison of CFD and experimental thermal mixing performance of the micromixers. The two micromixers of multistage Y-A shape were fabricated by varying the angles, 60° multistage Y-A-shaped and 45° Y-A-shaped micromixer. The Villermaux–Dushman results showed that 45° multistage Y-A-shaped micromixer had better mixing performance, and this is indicated by the segregation index of 0.015 as compared to the 60° multistage Y-A shape which had 0.02 for set 1 of the reagents in the Villermaux–Dushman protocols. More so, the mixing times of 45° multistage Y-A shape were lower than 60° multistage Y-A shape. From these results, it can be concluded that the size of the angle and the shape of the design of micromixer can affect the mixing performance. Table 2 also shows that the novel microreactor design had competitive mixing performance as shown by the low mixing time even at very low flowrates (laminar regime) compared to other studied microreactors which were operating at turbulent flows. The CFD and experimental results of thermal mixing further concur with the Dushman reactions results. The CFD results show that the 45° Y-A-shaped micromixer had better thermal mixing performance than the 60° Y-A-shaped micromixer. From the results, it showed that at 45° angle there were more eddies and vortices which indicates mixedness. In a nutshell, both the microreactors had good mixing due to the repeated multistage Y-A shape as seen by the very low segregation index in both the microreactors but 45° multistage Y-A shape had better performance. The main challenge encountered was that despite the 45° microreactor having better mixing performance, it had a higher pressure drop compared to 60° microreactors which will mean that more energy and power would be needed when operating the microreactor. This can be due to the constriction of sharp corners of the 45° angle in the micromixers. More future work is going to be done to improve the microreactors' design and innovate other mixing sources while reducing the effect of pressure drop due to the constricted 45° angle. In future this microreactor is to be tested for pharmaceutical reactions and photocatalytic reactions because of its transparent material which can allow light penetration into the flow channels.

References

1. Reckamp JM et al (2017) Mixing performance evaluation for commercially available micromixers using Villermaux–Dushman reaction scheme with the interaction by exchange with the mean model. Org Process Res Dev 21(6):816–820. https://doi.org/10.1021/acs.oprd.6b00332
2. Bem J, Yunho Y, Sung C, Im G (2017) Influence of adjusting the inlet channel confluence angle on mixing behaviour in inertial microfluidic mixers. Microfluid Nanofluid 21(7):1–9. https://doi.org/10.1007/s10404-017-1958-8
3. Lee CY, Fu LM (2018) Recent advances and applications of micromixers. Sens Actuators B Chem 259:677–702. https://doi.org/10.1016/j.snb.2017.12.034
4. Lv H, Chen X (2021) New insights into the mechanism of fluid mixing in the micromixer based on alternating current electric heating with film heaters. Int J Heat Mass Transf 181:121902. https://doi.org/10.1016/j.ijheatmasstransfer.2021.121902
5. Lv H, Chen X, Wang X, Zeng X, Ma Y (2022) A novel study on a micromixer with Cantor fractal obstacle through grey relational analysis. Int J Heat Mass Transf 183:122159. https://doi.org/10.1016/j.ijheatmasstransfer.2021.122159
6. Camarri S, Mariotti A, Galletti C, Brunazzi E, Mauri R, Salvetti MV (2020) An overview of flow features and mixing in micro T and arrow mixers. Ind Eng Chem Res 59(9):3669–3686. https://doi.org/10.1021/acs.iecr.9b04922
7. Lv P et al (2020) Mixing performance in T-shape microchannel at high flow rate for Villermaux–Dushman reaction. Microchem J 155:104662. https://doi.org/10.1016/j.microc.2020.104662
8. Lü Y, Zhu S, Wang K, Luo G (2016) Simulation of the mixing process in a straight tube with sudden changed cross-section. Chin J Chem Eng 24:711–718
9. Yao X, Zhang Y, Du L, Liu J, Yao J (2015) Review of the applications of microreactors. Renew Sustain Energy Rev 47:519–539. https://doi.org/10.1016/j.rser.2015.03.078
10. Abdulla Yusuf H, Hossain SMZ, Aloraibi S, Alzaabi NJ, Alfayhani MA, Almedfaie HJ (2022) Fabrication of novel microreactors in-house and their performance analysis via continuous production of biodiesel. Chem Eng Process Process Intensif 1720:108792. https://doi.org/10.1016/j.cep.2022.108792
11. Science N, Phenomena C, Lv H, Chen X, Zeng X (2021) Optimization of micromixer with Cantor fractal baffle based on simulated annealing algorithm. Chaos Solitons Fractals Interdiscip J Nonlinear Sci Nonequilib Complex Phenom 148:111048. https://doi.org/10.1016/j.chaos.2021.111048
12. Rahimi M, Valeh-e-Sheyda P, Parsamoghadam MA, Azimi N, Abidi H (2014) LASP and Villermaux/Dushman protocols for mixing performance in microchannels: Effect of geometry on micromixing characterization and size reduction. Chem Eng Process Process Intensif 85:178–186. https://doi.org/10.1016/j.cep.2014.09.001
13. Kashid MN, Renken A (2015) 4 Micromixing Devices 4.1
14. Commenge JM, Falk L (2011) Villermaux–Dushman protocol for experimental characterization of micromixers. Chem Eng Process Process Intensif 50(10):979–990. https://doi.org/10.1016/j.cep.2011.06.006
15. Pinot J, Commenge JM, Portha JF, Falk L (2014) New protocol of the Villermaux–Dushman reaction system to characterize micromixing effect in viscous media. Chem Eng Sci 118:94–101. https://doi.org/10.1016/j.ces.2014.07.010
16. Abiev RS, Makusheva IV (2022) Energy dissipation rate and micromixing in a two-step micro-reactor with intensively swirled flows
17. Lin Y, Yu X, Wang Z, Tu ST, Wang Z (2011) Design and evaluation of an easily fabricated micromixer with three-dimensional periodic perturbation. Chem Eng J 171(1):291–300. https://doi.org/10.1016/j.cej.2011.04.003
18. Zhang F, Marre S, Erriguible A (2019) Mixing intensification under turbulent conditions in a high pressure microreactor. Chem Eng J 382:122859. https://doi.org/10.1016/j.cej.2019.122859
19. Guichardon P, Falk L (2000) Characterisation of micromixing efficiency by the iodide-iodate reaction system. Part I: experimental procedure. Chem Eng Sci 55(19):4233–4243. https://doi.org/10.1016/S0009-2509(00)00068-3
20. Kajishima (2012) Computational fluid dynamics, applied computational fluid dynamics. In: Mechanical engineering series, pp 1–19
21. Moghimi M, Jalali N (2020) Design and fabrication of an effective micromixer through passive method. J Comput Appl Res Mech Eng 9(2):371–383. https://doi.org/10.22061/jcarme.2019.4018.1481
22. D'Orazio AO, Haelssig JB, Roberge DM, Macchi A (2021) Computational fluid dynamics simulation of pressure drop and macromixing in LL microreactors. Can J Chem Eng 99(8):1715–1732. https://doi.org/10.1002/cjce.24069
23. Silva JLD, Santana DHS (2022) Residence time distribution in reactive and non-reactive flow systems in micro and millidevices. Chem Eng Sci 248:117163. https://doi.org/10.1016/j.ces.2021.117163
24. Kotowicz M, Jasińska M (2021) An improved model for interpretation of micromixing experiment with iodide–iodate method and sulphuric acid. Chem Eng Res Des 165(3):270–279. https://doi.org/10.1016/j.cherd.2020.10.035
25. Yang M et al (2021) Mixing performance and continuous production of nanomaterials in an advanced-flow reactor. Chem Eng J 412:128565. https://doi.org/10.1016/j.cej.2021.128565
26. Lv P et al (2019) Mixing performance in T-shape microchannel at high flow rate for Villermaux–Dushman reaction. Microchem J 155:104662. https://doi.org/10.1016/j.microc.2020.104662
27. Wenzel D, Assirelli M, Rossen H, Lopattschenko M, Górak A (2018) On the reactant concentration and the reaction kinetics in the Villermaux–Dushman protocol. Chem Eng Process Process Intensif 130:332–341. https://doi.org/10.1016/j.cep.2018.06.022
28. Azimi N, Rahimi M, Hosseini F, Jafari O (2022) Investigation of mixing performance in a semi-active T-micromixer actuated by magnetic nanoparticles: characterization via Villermaux–Dushman reaction. Can J Chem Eng 2021:1–13. https://doi.org/10.1002/cjce.24377
29. Lafficher R, Digne M, Salvatori F, Boualleg M, Colson D, Puel F (2018) Influence of micromixing time and shear rate in fast contacting mixers on the precipitation of boehmite and NH4-dawsonite. Chem Eng Sci 175:343–353. https://doi.org/10.1016/j.ces.2017.10.011
30. Ouyang Y et al (2019) Micromixing efficiency optimization of the premixer of a rotating packed bed by CFD. Chem Eng Process Process Intensif 142(15):107543. https://doi.org/10.1016/j.cep.2019.107543
31. Yedala N, Kaisare NS (2021) Integration of heat recirculating microreactors with thermoelectric modules for power generation : a comparative study using CFD. React Chem Eng 6:2327–2341. https://doi.org/10.1039/d1re00382h
32. Liu G et al (2022) A novel design for split-and-recombine micromixer with double-layer Y-shaped mixing units. Sens Actuators A Phys 341:113569. https://doi.org/10.1016/j.sna.2022.113569
33. Su Y, Chen G, Kenig EY (2015) An experimental study on the numbering-up of microchannels for liquid mixing. Lab Chip 15(1):179–187. https://doi.org/10.1039/c4lc00987h
34. Rahimi M, Aghel B, Hatamifar B, Akbari M, Alsairafi AA (2014) CFD modeling of mixing intensification assisted with ultrasound wave in a T-type microreactor. Chem Eng Process Process Intensif 86:36–46. https://doi.org/10.1016/j.cep.2014.10.006

35. Li W, Xia F, Qin H, Zhang M, Li W, Zhang J (2019) Numerical and experimental investigations of micromixing performance and efficiency in a pore-array intensified tube-in-tube microchannel reactor. Chem Eng J 370:1350–1365. https://doi.org/10.1016/j.cej.2019.03.189
36. Woldemariam M, Filimonov R, Purtonen T, Sorvari J, Koiranen T, Eskelinen H (2016) Mixing performance evaluation of additive manufactured milli-scale reactors. Chem Eng Sci 152:26–34. https://doi.org/10.1016/j.ces.2016.05.030
37. Kashid M, Renken A, Kiwi-Minsker L (2011) Mixing efficiency and energy consumption for five generic microchannel designs. Chem Eng J 167(2–3):436–443. https://doi.org/10.1016/j.cej.2010.09.078